Genetic and functional insights into the fractal structure of the heart

Hannah V Meyer[1,11,+,C], Timothy JW Dawes[2,3,+], Marta Serrani[4,9,+], Wenjia Bai[5], Paweł Tokarczuk[2], Jiashen Cai[6,7], Antonio de Marvao[2], Albert Henry[12,15], R Thomas Lumbers[12,13,14], Jakob Gierten[16,17], Thomas Thumberger[17], Joachim Wittbrodt[17], James S Ware[2,3,18], Daniel Rueckert[5], Paul M Matthews[8], Sanjay K Prasad[3,18], Maria L Costantino[9,*], Stuart A Cook[2,3,6,10,*], Ewan Birney[11,*], and Declan P O'Regan[2,*,C]

[1]Cold Spring Harbor Laboratory, Simons Center for Quantitative Biology, USA
[2]MRC London Institute of Medical Sciences, Imperial College London, UK
[3]National Heart and Lung Institute, Imperial College London, UK
[4]Department of Chemical Engineering and Biotechnology, University of Cambridge, UK
[5]Department of Computing, Imperial College London, UK
[6]Duke–National University of Singapore, Singapore
[7]Department of Internal Medicine, Singapore Health Services, Singapore
[8]Department of Brain Sciences, Department of Medicine and UK Dementia Research Institute at Imperial College London, UK
[9]Department of Chemistry, Materials and Chemical Engineering, Politecnico di Milano, Italy
[10]National Heart Centre Singapore, Singapore
[11]European Molecular Biology Laboratory, European Bioinformatics Institute (EMBL-EBI), UK
[12]Institute of Health Informatics, University College London, UK
[13]Health Data Research UK, London, UK
[14]Barts Heart Centre, St. Bartholomew's Hospital, London, UK
[15]Institute of Cardiovascular Science, University College London, UK
[16]Department of Pediatric Cardiology, University Hospital Heidelberg, Heidelberg, Germany
[17]Centre for Organismal Studies, Heidelberg University, Heidelberg, Germany
[18]Cardiovascular Research Centre, Royal Brompton & Harefield NHS Foundation Trust, London, UK
[+]These authors contributed equally to this work
[*]These authors jointly supervised this work
[C]Corresponding authors

Contents

1 Supplementary Note

1.1 Mendelian randomisation

Mendelian randomization (MR) studies can be thought of as randomised control trials where genetic variants are used as instrumental variables (IV) to infer the effect of an exposure variable on the outcome variable. The randomization is described as Mendelian based on Mendel's laws of inheritance, i.e. the selection of alleles that an individual receives for a given genetic variant occurs at random during meiosis. This has two consequences, first the alleles are expected to be random with respect to confounders and second, they are causally upstream of the exposure traits. The effect of the exposure on outcome can then be inferred as the ratio of the genetic effect on the outcome over the genetic effect on the exposure.

In principle, there are two main types of MR analysis based on the study cohorts.[47] In one-sample MR studies both the genetic variant-exposure and -outcome effect size estimates are obtained from the same cohort. In two-sample MR studies, these effect size estimates are obtained in independent cohorts. In times of large biobanks where thousands of individuals are measured for hundreds of traits, intermediate set-ups exist, where there is sample overlap between the cohort in which the exposure association was measured and the cohort of the outcome association.

1.1.1 MR assumptions and biases

The basis of MR studies is 'vertical' pleiotropy i.e. the genetic variants under investigation are associated with both traits considered because one trait is causal to the other trait. In addition, Mendelian randomisation studies make the following main assumptions:

- the instrument is associated with the exposure (IV1 assumption),
- the instrument only influences the outcome through exposure and not through any other pathway (IV2 assumption),
- the instrument is not associated with confounders (IV3 assumption).

However, there is a second type of pleiotropy, 'horizontal' pleiotropy, where the genetic variant is associated with the outcome through confounders or a pathway other than the exposure. 'Horizontal' pleiotropy is a violation of the IV2 and IV3 assumption and has to be addressed when conducting MR analysis as it can lead to incorrect inference of the causal effects.[48,49] In addition, one has to further consider the nature of 'horizontal' pleiotropy: if the mean effect of the 'horizontal' pleiotropy is zero, it is considered balanced and will not effect the effect size estimate of the causal effect (but can effect its standard error). If the mean effect is unequal to zero, it is considered directional and the extend of pleiotropy can be estimated (see MR Egger below).

If there is sample overlap between the exposure and outcome cohort, the overlap can lead to the correlation of the uncertainty in the genetic variant-exposure association and the genetic variant-outcome association. This can cause a bias of the causal effect estimates towards the confounded observational association (especially for weak instruments due to Winner's curse[50]). IVs strongly correlated with the exposure (in practice defined as F statistic > 10) are less prone to this bias even in cohorts with overlapping samples.[51]

1.1.2 MR methods

A number of methods exist that can address violations to the IV assumptions outlined above. In the following, a selection of four methods used in this study are described in brief (for a comprehensive overview see[48–50]):

- **Inverse-variance weighted (IVW) linear regression.** If all IV are valid, IVW can be used to obtain an unbiased causal estimate of the exposure on the outcome. In IVW, the effect of the exposure on the outcome is estimated by linear regression of the effect size estimates of the genetic variant-exposure association on effect size estimates of the genetic variant-outcome association. The contribution of each IV to the overall effect is weighted by the inverse of the variance of the genetic variant-outcome effect and the intercept of the linear regression is constrained to pass through zero (no horizontal pleiotropy/balanced horizontal pleiotropy).[52]
- **MR Egger.** MR Egger works similar to IVW with the exception that the intercept is not restrained to pass through zero i.e. it allows to adjust for (unbalanced) pleiotropic effects. However, the effect estimates are only unbiased if the genetic variant-exposure associations and the pleiotropic effects are not correlated, i.e. the instrument strength is independent of direct effect (InSIDE assumption).[53]
- **Weighted median-based estimator.** The median-based estimator makes the assumption that the majority of IV are valid instruments. It is based on the ordered effect size estimate ratios for all IV-exposure to IV-outcome associations, weighted by standardised, inverse of the standard error of the Wald ratio estimated by the delta method (analogues to IVW). The weighted median-based estimator allows for unbalanced pleiotropy of the IVs and unlike MR Egger does not rely on the InSIDE assumption.[54]
- **Weighted mode-based estimator.** The mode-based estimator works based on cluster selection. It first clusters the IV into groups based on the similarity of the effect size estimates, and then selects the effect size estimate from the cluster with the largest number of IVs. The mode-based causal effect estimate is valid if the IVs in the largest cluster are valid.[55,56]

In addition to these methods, there are a number of statistics that can be used to evaluate the validity of a given method. Both the IVW and MR Egger make the no measurement error (NOME) assumption, i.e. they consider the variance of the

genetic variant-exposure association as negligible.[52] In IVW, the presence of large measurement error (violation of NOME) can lead to weak instrument bias. The strength of the instruments can be assessed with the F-statistic and as above for overlapping sample sizes, IVs which strongly correlated with the exposure (in practice defined as F statistic > 10) are less prone to this bias.[57] However, the F statistic is only a proxy for the true, but unknown parameter of interest, the F parameter. In addition to computing the cohort F statistic, one can also estimate a lower bound on the true F parameter as described in [58, Appendix A3]. For MR Egger and NOME violation, the causal effect size estimates can suffer from regression dilution bias which attenuates the causal effect estimate towards the null,[59] The MR Egger I^2 statistic can be calculated to evaluate the magnitude of dilution bias, e.g. an I^2 of 90% will lead to a 10% underestimation of the effect size.[59] The mode-based estimator can be implemented with or without the assumption of NOME.[55,56]

MR analysis can be used to infer whether there is a causality between exposure and outcome and which direction the effect takes i.e. exposure-outcome or outcome-exposure. With the MR Steiger test, the directionality can be assessed based in the absolute correlations of the genetic variants with the exposure and outcome (with Steiger's Z-test for correlated correlations within a population). Based on the Z statistic and the associated Steiger p-value one can then test at a predefined level α if one accepts the causal association for the model.[60]

1.1.3 Limitations in this study

We conducted MR analysis on the effect of FD on heart failure and dilated cardiomyopathy in the HERMES (The Heart Failure Molecular Epidemiology for Therapeutic Targets) and a DCM cohort, respectively (Figure 4c,d). To address potential biases in our analysis arising from potential violations in the instrumental variable assumptions we have conducted formal analysis to check for weak instrument bias, pleiotropy and dilution bias. We find evidence for weak pleiotropy effects in the MR on heart rate, but not on DCM (Supplementary Table 12). We only found very weak dilution bias (around 1.7%). We confirmed the direction of effect with the Steiger directionality test. To our knowledge, there is no sample overlap between individuals of the DCM study and the UK Biobank. However, there is a potential, minimal sample overlap between UK Biobank FD GWAS (18,096 samples) and cases in HERMES analysis. HERMES analysed a total of 47,309 heart failure cases, of which 6,504 were derived from UK Biobank (see Supplementary Tables document, sheet HERMES cohort characteristics). Of those heart failure cases in the UK Biobank a maximum of 185 samples had their MR taken, i.e. the potential overlap between samples of the FD GWAS and the cases in the HERMES Heart failure meta-analysis is 185/47, 309=0.4%. We estimated the effect this minimal overlap could have (potential for weak instrument bias) by computing the F statistics and lower bound estimation of the F parameter (Supplementary Table 11) and find that there is no sufficient evidence for weak instrument bias.

2 Supplementary Methods

All analysis in R conducted with R version $> 3.6.0$. All analyses in this study can be found here: `https://github.com/ImperialCollegeLondon/fractalgenetics/`.

Phenotyping

Participants: For UK Biobank, approximately 500,000 community-dwelling participants aged 40–69 years were recruited across the United Kingdom between 2006 and 2010.[61] Baseline summary characteristics of the cohort can be viewed on the UK Biobank data showcase (`http://www.ukbiobank.ac.uk`). Since 2014, a subset of participants are being recalled for CMR and a total of 19,701 consecutive CMR datasets were available at the start of this study, which were processed for our discovery cohort (May 2018 data release) and 7,192 for our validation cohort (December 2018 data release). All subjects provided written informed consent for participation in the study, which was also approved by the National Research Ethics Service (11/NW/0382). Our study was conducted under terms of access approval number 40616. The second validation cohort was drawn from the UK Digital Heart Project - a single-centre prospective study recruiting 2000 healthy volunteers by advertisement between February 2011 and July 2016 at the MRC London Institute of Medical Sciences. All subjects provided written informed consent for participation in the study, which was also approved by the National Research Ethics Service (09/H0707/69).

Assessment centre: For both populations an equivalent CMR protocol was followed to assess LV structure and function using conventional two-dimensional retrospectively-gated cine imaging on a 1.5T magnet.[62,63] A contiguous stack of images in the LV short-axis plane from base to apex was used for volumetric analysis and trabecular phenotyping. Images were curated on open-source databases.[64,65] Participants also underwent a resting 12 lead electrocardiogram which was automatically analysed using proprietary software (CardioSoft, GE Healthcare).

Image analysis: Segmentation of the short-axis cine images was performed using a fully convolutional network, a type of deep learning neural network, which predicts a pixelwise image segmentation by applying a number of convolutional filters onto each input image. The accuracy of image annotation using this algorithm is equivalent to expert human readers.[66] Label maps

were derived for all images in the cardiac cycle and LV volumes and mass were calculated according to standard guidelines,[67] and then indexed to body surface area (BSA) which was computed according to the Mosteller formula: $\sqrt{Weight \times Height}/60$, with weight in kg and height in cm. Lagrangian strain was calculated automatically using a validated 2D B-spline free-form deformation registration technique to estimate motion between consecutive cine frames.[68]

Fractal dimension (FD) - a scale-invariant measure of trabecular complexity - was derived using a fully-automated algorithm executed from Matlab (Mathworks, Natick, MA) using custom-written code (autoFD, in GitHub repository at automated-fractal-analysis). Short-axis CMR images were pre-processed with bicubic interpolation to 0.25 mm x 0.25 mm pixels to enable consistent analysis between subjects acquired at different native resolutions. For each slice, a region of interest was defined within the midwall of the LV myocardium between the automated endocardial and epicardial segmentations. Subsequent image processing consisted of bias-field correction using histogram stretching, applying a region-based level-set algorithm and then binarization of the blood pool and myocardium.[69] The trabecular borders were then detected using a Sobel filter and FD was calculated using a standard box-counting method in which the target image is overlain by a grid of known box size and the number of boxes containing non-zero image pixels is recorded. This process is repeated with box sizes between two pixels and 45% of the image size. Fractal dimension is defined as the negative gradient of an ordinary least-squares fit line to the logarithm of box size and box count. The FD values from all slices were interpolated using a Gaussian kernel local fit to a nine-slice template to allow comparison across subjects (see Extended Data Fig 2 and fractal-analysis-processing in the GitHub repository). The feasibility of extending fractal analysis to cardiac computed tomography (CT) was assessed on a publicly-available dataset of CT images in 20 individuals.[70]

For visual comparison of trabecular borders across individuals and genotypes, images were aligned by co-registering each ventricular segmentation to a common coordinate space and applying the same transformation to the corresponding greyscale image. For each slice, the trabecular and outer myocardial borders were extracted and their common center computed. The pixel positions of the edges were converted to radial coordinates (θ, r), with pre-defined step size of $\frac{\pi}{2000}$. The outer myocardial border was then registered to a circle with radius one. The radial translocation at each angle required for the outer border registration was then applied to trabecular outline, making the outlines comparable across individuals (in GitHub repository at fractal-analysis-processing and UK-Biobank-segmentations).

Pressure-volume loop analysis enables a detailed interpretation of cardiac physiology and ventricular work, but conventionally requires invasive catheterisation to obtain absolute pressure measurements which is not possible for population studies. Recently, a model-based framework combining non-invasive pressure measurements with CMR volumetry has been validated in a porcine model.[71] Here we take advantage of consecutive CMR imaging and peripheral pulse-wave analysis (Vicorder, Wuerzburg, Germany) for dynamic volumetric analysis and central pressure estimation respectively, to non-invasively model left ventricular pressure-volume relationships throughout the cardiac cycle. Peak systolic pressure and maximal aortic distension on axial cine imaging were assumed to be synchronous allowing LV volume at peak-systolic pressure to be assessed. The indexed volume difference between end-diastole and end-systole over a single cycle was defined as stroke volume index, and over a minute as cardiac index. Indexed systemic vascular resistance was defined as the difference between mean arterial pressure and central venous pressure divided by cardiac index. In the absence of invasive catheter data, a value of 5mmHg for central venous pressure was assumed. LV diastolic pressures were assumed to be normal and rise during diastole from 4mmHg to 8mmHg at end-diastole.[72] To understand the association of FD with pressure-volume dynamics, the mean ventricular FD value was associated with pressure and volume measurements during diastole and systole using linear regression, while controlling for contractility, systemic vascular resistance, trabecular mass and heart rate. Using this model, pressure-volume loops at comparable FD to the finite element model were plotted (in pv-loops of GitHub repository).

Genotyping

Discovery cohort

UK Biobank genotypes release version 3 (in GRCh37 coordinates) were used in the genetic association studies, for computing genetic principal components and for the Mendelian randomisation analyses. First, only unrelated or distantly related individuals were selected for further analysis based on the estimated identity of descent (IBD) provided by UK Biobank (via 'ukbgene rel key.enc'). Selection of individuals from families is optimised to retain as many unrelated individuals as possible in the study i.e. in family trios only parents would be considered for analysis. For computation of genetic principal components, genotypes were formated into plink binary format,[73] LD pruned (flag '–indep-pairwise 50kb 1 0.8') and a minor allele frequency (MAF) threshold of 1% applied. The filtered dataset was used with flashpca version 2,[74] to compute the first 50 principal components of the UK Biobank genotypes. Population substructures arising due to different ethnic origins of samples were examined by comparing the UK Biobank genotypes to genotypes from the HapMap Phase III study,[75] for four ethnic populations (with subpopulations, Extended Data Fig 1a). Download of reference data sets, fusion of UK Biobank and Hapmap data sets and PCA selection was done as described in plinkQC.[76] Individuals that clustered with the main cluster of the PC1/PC2 plot, which was also the position of the main cluster of HapMap III individuals of European ancestry were kept for further analyses,

as is standard in GWAS analysis to model a well mixed population. The genotypes of the remaining unrelated individuals were filtered for genetic variants that passed a MAF threshold of 0.1% and an imputation INFO threshold of > 0.4. For association analysis this was achieved by providing a variant ID list with variant MAF > 0.001 to BGENIE. After genotyping and phenotyping quality control, the discovery cohort was composed of 18,096 individuals and 14,134,301 genetic variants. All relevant analysis in UK-Biobank and ancestry in the GitHub repository.

Replication cohorts

UK Biobank replication cohort. The UK Biobank released an additional 7,192 CMR images on in December 2018. We applied the same genotyping and phenotyping quality control as described above for the UK Biobank discovery cohort and obtained a replication cohort of 6,536 individuals and 14,069,398 genetic variants.

UK Digital Heart cohort. UK Digital Heart project genotyping and genotype calling were carried out at the Genotyping and Microarray facility at the Wellcome Sanger Institute, UK and Duke-NUS Medical School, Singapore. Genotypes were assessed in five batches using Illumina HumanOmniExpress-12v1-1 (Sanger, two batches), Illumina HumanOmniExpress-24v1-0 (Duke-NUS, two batches) and Illumina HumanOmniExpress- 24v1-1 chips (Duke-NUS). Genotypes were called via the GenCall software.[77] For batches run on the same platform, genotype signals were combined and called in a single analysis, leading to three independent genotype batches. In order to avoid batch effects in genotype calling based on the probe sequences, probes targeting the same genotypes were checked for the concordance of the capture sequence. Genotyping probes common to all three platforms were selected and a common genotype dataset generated using PLINK v1.9,[73] with plinkQC[76] applied to assess the quality of the genotyping on a per-individual and per-marker level. In summary, the per-individual quality control included the identification of individuals with discordant sex information, missing genotype rates (more than 3% of genotypes not called) and heterozygosity rate outliers (three standard deviations outside of the mean heterozygosity rate). Population substructures arising due to different ethnic origins of samples were examined by comparing the sample genotypes to genotypes from the HapMap Phase III study,[75] for four ethnic populations (with subpopulations, Extended Data Fig 1b). Individuals that clustered with the main cluster of the PC1/PC2 plot, which was also the position of the main cluster of HapMap III individuals of European ancestry were kept for further analyses, as is standard in GWAS analysis to model a well mixed population. The per-marker quality control included filtering of genotypes with missing call rate in more than 1% of the samples and genotypes which significantly deviate from Hardy-Weinberg equilibrium (HWE, $p < 0.001$). After removing samples and genotypes that failed quality control, we confirmed that any pattern of missing genotype information was not batch-specific. To analyse these patterns, each pair-wise combination of batches was treated as a case-control set-up and the differential missingness of genotypes computed. All variants with significant differential missingness ($p < 10^{-5}$) were removed from the dataset. After quality control, genotypes were phased and imputed to the combined 1000 Genomes[78] and UK10K[79] reference panel using SHAPEIT (version 2.r727)[80] and IMPUTE2 (version 2.3.0).[81] The window size for phasing was set to 2Mb, and the number of conditioning states per genotype to 200. The imputation interval was set to 3Mb, with a buffer region of 250kb on either side of the analysis interval. The effective population size was set to 20,000 and the number of reference haplotypes to 1,000. For other non-specified parameters the default values were used. Analysis of UK Biobank cohort in UK-Biobank-ancestry and UK-BioBank-phenotypes, of UK Digital Heart cohort in digital-heart-genotypes and digital-heart-phenotypes in the GitHub repository).

LD reference

We generated a LD reference for downstream filtering of association results based on the quality controlled genotypes described above (non related, European, MAF > 0.001, INFO > 0.4). For each variant we computed all variants with r2 > 0.05 in a LD window of 250 kb using the following plink version 2 command: 'plink2 –bfile input –indep-pairwise 50kb 1 0.8'.

Association analysis

Analysis are in UK-Biobank-association for UK Biobank and in digital-heart-association for the UK Digital Heart cohort on GitHub.

Univariate association: Genetic association of trabecular FD for samples passing genotype and phenotype quality control (UK Biobank discovery: 18,096, UK Biobank replication: 6,536, UK Digital Heart project: 1,129) were conducted using BGENIE v1.3 (`https://jmarchini.org/bgenie`).[82] In the UK Biobank discovery cohort, we conducted univariate GWAS on the interpolated FD measurements per slice (9 independent GWAS) and the mean FD measurements per ventricular region (3 independent GWAS of basal, mid-ventricular and apical FD), by fitting an additive model of association at each variant based on the genotype dosage of the imputed genotypes. In addition, we included sex, age, height, weight, BMI and principal components of the genotypes as co-variates in the model. To test for the effect of ventricular size, we conducted analogous GWAS in the discovery cohort, where we additionally included left ventricular end-diastolic volume and longitudinal strain as a co-variates. The univariate GWAS were adjusted for multiple-hypothesis testing by estimating the effective number of

phenotype-association tests conducted[83]. The effective number of tests is estimated based on the eigenvalues $\mathbf{u}$ of the empirical trait-by-trait correlation matrix $\mathbf{C}$. The effective number of tests is $T_{eff} = \frac{\sum_{i=1}^{n}\sqrt{u_i^2}}{\sum_{i=1}^{n} u_i}$, where n is the number of GWAS conducted i.e. $n = 9$ and $n = 3$ for per-slice and per-region GWAS, respectively. The p-values of these GWAS were multiplied by the effective number of tests and the $min(p_{adjust}, 1)$ reported. Associations were considered significant if $p_{adjust} < 5 \times 10^{-8}$. The association tests in both replication cohorts used the same analysis setting and parameters as in the discovery cohort.

Multi-trait meta-analysis: We used an approximate, multi-trait meta-analysis[84] based on the univariate signed t-statistics of the 14,134,301 genetic variants for the nine per-slice FD GWAS. The multivariate test statistic is computed as $t_{meta} = \mathbf{t}_i^T \mathbf{V}^{-1} \mathbf{t}_i$, where $\mathbf{t}_i$ is the vector of the signed t-values of variant$_i$ for the nine FD measurements, $\mathbf{t}_i^T$ is a transpose of vector $\mathbf{t}_i$, $\mathbf{V}^{-1}$ is the inverse of the trait-by-trait correlation matrix $\mathbf{V}$. $\mathbf{V}_{i,j}$ for each trait-trait pair is the correlation over the 14,134,301 estimated signed t-values of the two traits. t_{meta} is approximately chi-square distributed with 9 degrees of freedom and tests the null hypothesis that the genetic variant tested does not affect any of the nine traits. We used the LD reference panel described above to clump all SNPs with $p < 5 \times 10^{-8}$ into one SNP per locus, keeping the SNP with the lowest p-value.

Validation analysis: The effect size estimates of the FD GWAS of the discovery cohort (UK Biobank) and the corresponding associations of the validation cohorts (UK Biobank validation cohort with 6,536 individuals, UK Digital Heart project with 1,129 individuals) were tested for concordance. For each locus in the discovery cohort that showed association with $p_{adjust} < 5 \times 10^{-8}$, the genetic variant with the lowest p-value was selected. This selection was done for each univariate per-slice GWAS. The same loci-slice associations were selected in the validation cohort. Variant rs71394376 is not present in UK Digital Heart genotypes and concordance was only tested at 15 out of 16 associated loci. The effect size estimated for the selected genetic variants in the discovery and validation data set were then compared for concordance, i.e. same effect size direction. To evaluate if the observed concordance was likely to arise by chance alone, an empirical p-value for concordance was estimated by randomly selecting slice-variant associations with a slice distribution as observed in the discovery associations. In each random selection step, the concordance of the observed and randomly selected slice effect size estimates was computed. The number of times the random concordance was greater or equal than the observed concordance was divided by the number of random selections (10,000) to yield the empirical p-value.

Variant annotations

Variant annotations from previous studies were retrieved from the GWAS catalogue [85, accessed 28 January 2019] for the GWAS annotations, Open targets genetics v0.3.2 (https://genetics.opentargets.org/)[86] for the nearest protein coding gene and PheWAS annotations, the ENSEMBL regulatory build[87] and GTEx v7 (https://gtexportal.org/home/, accessed 28 January 2019) for the expression quantitative trait loci annotations. Annotations were reported when they passed the platform-specific significant thresholds (0.05 FDR on GTEx) or the commonly used GWAS threshold of 5×10^{-8}. For variants annotated in GTEx, we downloaded the baseline gene expression counts of the associated genes and tissues from https://www.ebi.ac.uk/gxa/home by querying: gene name AND tissue AND species, e.g. GOSR2 AND heart component AND Homo sapiens. Cluster plots of genotype calls for all genotyped lead variants and their LD proxies were generated with *ScatterShot* (http://mccarthy.well.ox.ac.uk/static/software/scattershot; Supplementary Table 14 and Supplementary Fig 1).

Functional enrichment analysis

We used GARFIELD version 2[88] for functional enrichment analyses of genetic variants with multi-trait GWAS p-value $< 10^{-6}$. GARFIELD accounts for LD structure and local gene density and derives functional enrichment scores (odds ratios) by fitting a logistic regression model. The GARFIELD software package and pre-computed data for samples of European ancestry (LD and annotation data, minor allele frequencies of genetic variants and their distances to nearest transcription start site) were downloaded from https://www.ebi.ac.uk/birney-srv/GARFIELD. GARFIELD was run as described in the user manual at https://www.ebi.ac.uk/birney-srv/GARFIELD/documentation-v2/GARFIELD-v2.pdf. Annotation results (.perm GARFIELD output file) were filtered for input GWAS threshold (PThres $< 10^{-6}$) and significance of enrichment (EmpPval $< 10^{-3}$).

Genomewide trait and disease correlation

We analysed the genetic correlation of the basal, mid and apical trabeculation phenotypes with all available traits on LDhub, a centralized database of summary-level GWAS results for 732 traits (accessed August 2019, http://ldsc.broadinstitute.org/ldhub/[89]). LDhub uses cross-trait LD score regression to estimate the genetic correlation between two traits z_1 and z_2. It uses the amount of genetic variation tagged by a genetic variant j (its LD score l_j) and regresses the LD scores against the product of the two traits $z_1 z_2$. The slope of this regression estimates the genetic covariance between traits z_1 and z_2. The normalisation of the genetic covariance by the square root of the product of the traits' additive SNP heritabilities h_1^2 and h_2^2

yields the genetic correlation between the traits.[90] Prior to upload to LDhub, we reduced the trabeculation summary statistics to the number of variants included on LDhub (1,208,036 variants, as described in the LDhub test center). The additive heritability estimates were extracted from the -h2.log file, the genetic correlation results from the rg.results.csv file. Results were depicted in a PheWAS manhattan plot. The remainder of the analysis was focused on the genetic correlation of trabeculation phenotypes on cardiac and cardiovascular traits, selected by manual inspection of all LDhub traits (selected traits in Supplementary Table 13).

Trabeculation phenotypes and associated loci in dilated cardiomyopathy

The dilated cardiomyopathy (DCM) cohort were prospectively recruited to the NIHR Biobank at the Royal Brompton Hospital, London. All patients underwent cardiac phenotyping with either CMR or transthoracic echocardiography, with DCM diagnosed based on evidence of left ventricular dilatation and systolic impairment with reference to age, gender and body surface area adjusted nomograms. All participants gave written informed consent and the study was approved by the relevant regional research ethics committees. Demographic and clinical characteristics are provided in Extended Data Table 1.

We conducted a logistic regression of loci associated with trabecular phenotypes in the DCM patients and healthy volunteers of the UK Digital Heart Project (1,136 individuals as described in Genotyping replication cohort). We tested all genetic variants and variants in LD ($r^2 > 0.1$) at the 16 loci associated with trabeculation (1,015 variants). We excluded any samples that did not cluster with the European samples of the HapMap consortium and filtered for unrelated individuals (see Genotyping replication cohort; *plinkQC*[76]). We prioritised retaining DCM cases compared to controls in pairs of related individuals. We filtered any genetic variants that showed differential genotype missingness (p-value < 0.01 in cases versus controls using PLINK 1.9[73] '–test-missing'. 510 DCM cases and 1,134 healthy volunteers and 1,005 variants passed the quality control. They were analysed in a logistic regression model with allele dosage encoding for genetic variant effect, sex and age as covariates and an adaptive permutation approach for the genetic variant effect to obtain empirical p-values (using sample label swapping described here `http://zzz.bwh.harvard.edu/plink/perm.shtml`): 'plink –logistic perm'. In addition, we jointly modeled the per-slice FD phenotypes of DCM patients (307 patients) and UK Biobank discovery cohort as the response variable in a linear mixed model with study (DCM or UK Biobank) as fixed effect and slice (1-9) as random effect (R package *nlme*, v3.1-140.). Analysis can be found in digital-heart-association on GitHub.

Trabeculae associated loci in heart failure

GWAS summary data were provided by the Heart Failure Molecular Epidemiology for Therapeutic Targets (HERMES) Consortium for 47,309 cases of heart failure and 930,014 controls of European ancestry from 26 cohorts (comprising 29 distinct datasets, cohort characteristics in Supplementary Data 5, obtained from Supplementary Table 17[91]), with either a population-based or case-control study design. A detailed description of the study is reported elsewhere.[91] In brief, cases were defined by the clinical diagnosis of heart failure and no restrictions on aetiology or morpho-functional phenotypes were made. Following genotyping using high-density arrays and genotype and pre-imputation quality control, study-level genotype data were imputed using reference panels from the 1000 Genomes Project (60%), Haplotype Reference Consortium (35%) or population-specific reference data (5%). Association testing for single nucleotide polymorphisms was then performed using logistic regression including age, sex and principal components as covariates, and assuming additive genetic effects. Meta-analysis of GWAS estimates was performed using fixed-effect inverse variance weighted analysis, implemented in METAL (released March 25, 2011). The linkage disequilibrium score regression (LDSC) intercept, implemented using LDSC v1.0.022, was estimated at 1.0069, suggesting no inflation of the test statistic due to cryptic population structure. The summary statistics for the HERMES consortium are publicly available at: http://www.broadcvdi.org/.

Mendelian randomisation analyses

Mendelian randomisation (MR) analysis was performed using all independent, genetic loci (see Association analysis: Multi-trait meta-analysis) with per-slice, univariate GWAS adjusted p-value $p_{adjust} = p \times T_{eff} < 5 \times 10^{-8}$. For variants associated with FD in multiple slices, only the slice association with the lowest p-value was used. All variants available in the outcome studies were considered. All MR analyses were conducted using the R-package *TwoSampleMR* (`https://github.com/MRCIEU/TwoSampleMR`, version 0.5.1).[56] Two-sample MR studies with the FD associations described above as the exposure variables and the association of those loci with mixed aetiology heart failure (HERMES consortium, see above and summary of cohort characteristics in Supplementary Data 5) and DCM (DCM cohort, see above) as outcomes were conducted (harmonised, ie effect allele matched input data for MR in Supplementary Data 6). The effect size of trabeculation on these traits was estimated with *TwoSampleMR* functions for weighted median, weighted mode, inverse variance weighting and MR-Egger. In addition, the Steiger test for directionality,[60] leave-one-out sensitive analysis to determine the influence of single genetic variants on the overall effect, MR pleiotropy analyses and I^2 analysis for assessing bias in MR-Egger analysis were conducted.[59] For details refer to Supplementary Note 1.1:Mendelian randomisation.

Finite element modelling

We used a biomechanical model to assess the causative effect of varying trabecular morphology on cardiovascular physiology. To achieve this we compared ventricular behaviour with different degrees of trabecular complexity in the non-compact layer while keeping the total ventricular mass constant. A geometric model of the left ventricle was represented by a symmetric truncated ellipsoid in series with a pre-load and after-load circuit. The simulation was calibrated to approximate median physiological variables observed in the UK Biobank population. Trabeculae were modelled as cylindrical strands orientated in the endocardial long-axis.[92,93] Fractal dimension was calculated from cross-sections of the left ventricular model using the same methodology as for clinical imaging. We recorded the consequent effect of changing trabecular morphology on ventricular volume, contractility and blood pressure at steady state.

The ventricular model replicated *ex vivo* fibre orientations,[94] and accounted for both active and passive material properties of the myocardium using a hyperelastic anisotropic constitutive framework. Specifically, the strain energy function ψ selected to model the cardiac tissue is $\psi = C_{10}(\bar{I}_1 - 3) + \frac{k_1}{2k_2}[exp(k_2(\bar{I}_4 - 1)^2) - 1]$, where $\bar{I}_1$ and $\bar{I}_4$ are the first and fourth invariant of the modified Cauchy-Green tensor $\bar{\mathbf{C}}$ and C_{10}, k_1 and k_2 are material parameters. Boundary conditions for the simulations included constraints on rigid motion and displacements of the ventricular base with implementation of a pre-load (defining left atrial pressure and inflow resistance) and after-load circuit (defining right atrial pressure, aortic/peripheral resistance, and capacitance). The models were discretized to allow finite element analyses with eight-node hexahedral elements into more than 10^4 elements using Ansys Meshing (ANSYS Inc., Canonsburg, PA, USA). The property of differential fibre orientation within the ventricular wall, in which the sheets of muscle fibres describe a consistent helical pattern, was preserved by considering ventricular dynamics in nine separate myofibrillar sheets,[94,95] with linearly varying fibre orientation from +80 to -80 degrees with respect to the long-axis. Myocyte contraction in systole was simulated by changing the myocyte stiffness parameters to emulate the observed force/time data from cardiac fibres in response to intracellular calcium variation.[96] Torsional motion was modelled by myocyte contraction patterns creating a realistic counter-clockwise apical rotation with respect to the base.[97–99] The finite element problem was solved by means of the commercial code Abaqus (Abaqus 6.14, SIMULIA, Dessault Systemes). Simulations were performed under the assumption of quasi-static processes, so neglecting any inertia effects. Pressure-volume data are reported during steady state after a minimum of five simulated cardiac cycles. For details about the model parameters please refer to Supplementary Table 15 and Supplementary Table 16 and Finite-element-modelling on GitHub.

Medaka experiments

Fish maintenance: The wild-type Cab strain and a *myl7::EGFP* fluorescent cardiac reporter line were used. All fish are maintained in closed stocks at Heidelberg University. Medaka (*Oryzias latipes*) husbandry (permit number 35–9185.64/BH Wittbrodt) was performed according to local animal welfare standards (Tierschutzgesetz §11, Abs. 1, Nr. 1) and in accordance with European Union animal welfare guidelines.[100] The fish facility is under the supervision of the local representative of the animal welfare agency. Medaka was raised and maintained as described previously.[101] Unblinded analysis was performed using a sample size sufficient for descriptive analysis. All data were generated on embryos, whose sex is not discernible by external features.

sgRNA target site selection: *gosr2* (ENSORLG00000004536) sgRNAs, *mtss1* (ENSORLG00000004945) sgRNAs, and *tnnt2a* (ENSORLG00000024544) sgRNAs were designed with CCTop as described previously,[102] on the medaka genome in Ensembl release 95 (Japanese medaka HdrR assembly ASM223467v1, INSDC Assembly GCA_002234675.1, Jul 2017). Target sites and oligonucleotudes for sgRNA cloning in Supplementary Tables 17 and 18. Cloning of sgRNA templates and in vitro transcription was performed as detailed in Stemmer et al. (2015).[102]

***In vitro* transcription of mRNA:** The plasmids pCS2+(Cas9) and pCS2+(H2A-mCherry) were linearized using NotI, and mRNA in vitro transcription was performed using the mMessage mMachine SP6 Kit (ThermoFisher Scientific, AM1340).

Microinjection and screening: For the CRISPR-Cas9 experiments, medaka zygotes were injected with 150 ng/μl of Cas9 mRNA and 15 ng/μl of each sgRNA per gene as well as 10 ng/μl H2A-mCherry mRNA. Injected embryos were maintained at 22-28°C in embryo rearing medium (ERM, 17 mM NaCl, 40 mM KCl, 0.27 mM $CaCl_2$, 0.66 mM $MgSO_4$, 17 mM Hepes). One day post fertilization, embryos were selected for H2A-mCherry expression. Phenotypes of CRISPR-Cas9-mediated knock out of *gosr2*, *mtss1*, *tnnt2a*, and control injection (H2A-mCherry) were assessed at 4 DPF separately by two investigators.

Imaging: BF images were acquired using a Nikon SMZ18 equipped with a lumencor SOLA SE light source, a Nikon DS-Fi2 camera, and Software NIS-Elements v.4.20.

LSM was carried out on a 16x multiview selective plane illumination microscope (MuVi-SPIM).[103] Embryos were anesthetized with 200 mg/l tricaine and electromechanically decoupled with 30 mM 2,3-butanedione 2-monoxime (BDM). After complete inhibition of cardiac contraction, embryos were mounted with 1% low-melting agarose (LMA) containing 200 mg/l tricaine and 30 mM BDM into custom FEP tubes connected to a glass capillary. FEP-glass-capillaries were washed with

70% ethanol before usage. Entire heart volumes were acquired with 488 nm illumination, a 525/50 nm bandpass filter, and a z step size of 2 μm. Surface rendering was performed with UCSF Chimera (1.11).

References

47. Lawlor, D. A. Commentary: Two-sample Mendelian randomization: opportunities and challenges. *Int J Epidemiol* **45**, 908–15 (2016).

48. Davey Smith, G. & Hemani, G. Mendelian randomization: genetic anchors for causal inference in epidemiological studies. *Hum Mol Genet* **23**, R89–R98 (2014).

49. Haycock, P. C. *et al.* Best (but oft-forgotten) practices: the design, analysis, and interpretation of Mendelian randomization studies. *Am J Clin Nutr* **103**, 965–978 (2016).

50. Holmes, M. V., Ala-Korpela, M. & Smith, G. D. Mendelian randomization in cardiometabolic disease: challenges in evaluating causality. *Nat Rev Cardiol* **14**, 577–590 (2017).

51. Pierce, B. L. & Burgess, S. Efficient Design for Mendelian Randomization Studies: Subsample and 2-Sample Instrumental Variable Estimators. *Am J Epidemiol* **178**, 1177–1184 (2013).

52. Burgess, S., Butterworth, A. & Thompson, S. G. Mendelian Randomization Analysis With Multiple Genetic Variants Using Summarized Data. *Genet Epidemiol* **37**, 658–665 (2013).

53. Bowden, J., Davey Smith, G. & Burgess, S. Mendelian randomization with invalid instruments: effect estimation and bias detection through Egger regression. *Int J Epidemiol* **44**, 512–525 (2015).

54. Bowden, J., Davey Smith, G., Haycock, P. C. & Burgess, S. Consistent Estimation in Mendelian Randomization with Some Invalid Instruments Using a Weighted Median Estimator. *Genet Epidemiol* **40**, 304–314 (2016).

55. Hartwig, F. P., Davey Smith, G. & Bowden, J. Robust inference in summary data Mendelian randomization via the zero modal pleiotropy assumption. *Int J Epidemiol* **46**, 1985–1998 (2017).

56. Hemani, G. *et al.* The MR-Base platform supports systematic causal inference across the human phenome. *eLife* **7**, e34408 (2018).

57. Burgess, S., Thompson, S. G. & CRP CHD Genetics Collaboration. Avoiding bias from weak instruments in Mendelian randomization studies. *Int J Epidemiol* **40**, 755–764 (2011).

58. Burgess, S., Davies, N. M. & Thompson, S. G. Bias due to participant overlap in two-sample Mendelian randomization. *Genet Epidemiol* **40**, 597–608 (2016).

59. Bowden, J. *et al.* Assessing the suitability of summary data for two-sample Mendelian randomization analyses using MR-Egger regression: the role of the I2 statistic. *Int J Epidemiol* **45**, 1961–1974 (2016).

60. Hemani, G., Tilling, K. & Davey Smith, G. Orienting the causal relationship between imprecisely measured traits using GWAS summary data. *PLoS Genet* **13**, e1007081 (2017).

61. Sudlow, C. *et al.* UK biobank: an open access resource for identifying the causes of a wide range of complex diseases of middle and old age. *PLoS Med* **12**, 1–10 (2015).

62. Petersen, S. E. *et al.* UK biobank's cardiovascular magnetic resonance protocol. *J Cardiovasc Magn Reson* **18**, 8 (2016).

63. de Marvao, A. *et al.* Population-based studies of myocardial hypertrophy: high resolution cardiovascular magnetic resonance atlases improve statistical power. *J Cardiovasc Magn Reson* **16**, 16 (2014).

64. Woodbridge, M., Fagiolo, G. & O'Regan, D. P. MRIdb: medical image management for biobank research. *J Digit Imaging* **26**, 886–90 (2013).

65. Marcus, D. S., Olsen, T. R., Ramaratnam, M. & Buckner, R. L. The Extensible Neuroimaging Archive Toolkit: an informatics platform for managing, exploring, and sharing neuroimaging data. *Neuroinformatics* **5**, 11–34 (2007).

66. Bai, W. *et al.* Automated cardiovascular magnetic resonance image analysis with fully convolutional networks. *J Cardiovasc Magn Reson* **20**, 65 (2018).

67. Schulz-Menger, J. *et al.* Standardized image interpretation and post processing in cardiovascular magnetic resonance: Society for Cardiovascular Magnetic Resonance (SCMR) board of trustees task force on standardized post processing. *J Cardiovasc Magn Reson* **15**, 35 (2013).

68. Puyol-Antón, E. *et al.* Fully automated myocardial strain estimation from cine MRI using convolutional neural networks. In *2018 IEEE 15th International Symposium on Biomedical Imaging (ISBI 2018)*, 1139–1143 (2018).

69. Li, C. *et al.* A level set method for image segmentation in the presence of intensity inhomogeneities with application to mri. *IEEE Trans Image Process* **20**, 2007–16 (2011).

70. Zhuang, X. *et al.* Evaluation of algorithms for multi-modality whole heart segmentation: An open-access grand challenge. *Med Imag Anal* **58**, 101537 (2019).

71. Seemann, F. *et al.* Noninvasive quantification of pressure-volume loops from brachial pressure and cardiovascular magnetic resonance. *Circ Cardiovasc Imaging* **12**, e008493 (2019).

72. Bouchard, R. J., Gault, J. H. & Ross, J., J. Evaluation of pulmonary arterial end-diastolic pressure as an estimate of left ventricular end-diastolic pressure in patients with normal and abnormal left ventricular performance. *Circulation* **44**, 1072–9 (1971).

73. Chang, C. C. *et al.* Second-generation PLINK: rising to the challenge of larger and richer datasets. *GigaScience* **4**, 7 (2015).

74. Abraham, G., Qiu, Y. & Inouye, M. FlashPCA2: principal component analysis of Biobank-scale genotype datasets. *Bioinformatics* **33**, 2776–2778 (2017).

75. The International HapMap Consortium. Integrating common and rare genetic variation in diverse human populations. *Nature* **467** (2010).

76. Meyer, H. V. R package: plinkQC. https://cran.r-project.org/web/packages/plinkQC/ (2018).

77. Teo, Y. Y. *et al.* A genotype calling algorithm for the Illumina BeadArray platform. *Bioinformatics* **23**, 2741–6 (2007).

78. 1000 Genomes Project Consortium. A global reference for human genetic variation. *Nature* **526**, 68–74 (2015).

79. UK10K Consortium. The UK10K project identifies rare variants in health and disease. *Nature* **526**, 82–90 (2015).

80. Delaneau, O., Zagury, J.-F. & Marchini, J. Improved whole-chromosome phasing for disease and population genetic studies. *Nat Methods* **10**, 5–6 (2013).

81. Howie, B., Marchini, J. & Stephens, M. Genotype imputation with thousands of genomes. *G3* **1**, 457–70 (2011).

82. Bycroft, C. *et al.* The UK biobank resource with deep phenotyping and genomic data. *Nature* **562**, 203–209 (2018).

83. Galwey, N. W. A new measure of the effective number of tests, a practical tool for comparing families of non-independent significance tests. *Genet Epidemiol* **33**, 559–68 (2009).

84. Bolormaa, S. *et al.* A multi-trait, meta-analysis for detecting pleiotropic polymorphisms for stature, fatness and reproduction in beef cattle. *PLoS genetics* **10**, e1004198 (2014).

85. Buniello, A. *et al.* The NHGRI-EBI GWAS Catalog of published genome-wide association studies, targeted arrays and summary statistics 2019. *Nucleic Acids Res* **47**, D1005–D1012 (2019).

86. Carvalho-Silva, D. *et al.* Open Targets Platform: new developments and updates two years on. *Nucleic Acids Res* **47**, D1056–D1065 (2018).

87. Zerbino, D. R., Wilder, S. P., Johnson, N., Juettemann, T. & Flicek, P. R. The Ensembl regulatory build. *Genome Biol* **16**, 56 (2015).

88. Iotchkova, V. *et al.* GARFIELD classifies disease-relevant genomic features through integration of functional annotations with association signals. *Nat Genet* **51**, 343–353 (2019).

89. Zheng, J. *et al.* LD Hub: a centralized database and web interface to perform LD score regression that maximizes the potential of summary level GWAS data for SNP heritability and genetic correlation analysis. *Bioinformatics* **33**, 272–279 (2017).

90. Bulik-Sullivan, B. *et al.* An atlas of genetic correlations across human diseases and traits. *Nat Genet* **47**, 1236–1241 (2015).

91. Shah, S. *et al.* Genome-wide association and Mendelian randomisation analysis provide insights into the pathogenesis of heart failure. *Nat Commun* **11**, 163 (2020).

92. Gati, S. *et al.* Increased left ventricular trabeculation in highly trained athletes: do we need more stringent criteria for the diagnosis of left ventricular non-compaction in athletes? *Heart* **99**, 401–8 (2013).

93. Tamborini, G. *et al.* Incidence and characteristics of left ventricular false tendons and trabeculations in the normal and pathologic heart by second harmonic echocardiography. *J Am Soc Echocardiogr* **17**, 367–74 (2004).

94. Streeter, J., D. D., Spotnitz, H. M., Patel, D. P., Ross, J., J. & Sonnenblick, E. H. Fiber orientation in the canine left ventricle during diastole and systole. *Circ Res* **24**, 339–47 (1969).

95. Lombaert, H. *et al.* Human atlas of the cardiac fiber architecture: study on a healthy population. *IEEE Trans Med Imaging* **31**, 1436–47 (2012).

96. Backx, P. H., Gao, W. D., Azan-Backx, M. D. & Marban, E. The relationship between contractile force and intracellular [Ca2+] in intact rat cardiac trabeculae. *J Gen Physiol* **105**, 1–19 (1995).

97. Buckberg, G. *et al.* Ventricular torsion and untwisting: further insights into mechanics and timing interdependence: a viewpoint. *Echocardiography* **28**, 782–804 (2011).

98. Takeuchi, M., Otsuji, Y. & Lang, R. M. Evaluation of left ventricular function using left ventricular twist and torsion parameters. *Curr Cardiol Rep* **11**, 225–30 (2009).

99. Carreras, F. *et al.* Left ventricular torsion and longitudinal shortening: two fundamental components of myocardial mechanics assessed by tagged cine-MRI in normal subjects. *Int J Cardiovasc Imaging* **28**, 273–84 (2012).

100. Bert, B. *et al.* Considerations for a European animal welfare standard to evaluate adverse phenotypes in teleost fish. *EMBO J* **35**, 1151–4 (2016).

101. Gierten, J. *et al.* Automated high-throughput heartbeat quantification in medaka and zebrafish embryos under physiological conditions. *Sci Rep* **10**, 2046 (2020).

102. Stemmer, M., Thumberger, T., Del Sol Keyer, M., Wittbrodt, J. & Mateo, J. L. CCTop: An Intuitive, Flexible and Reliable CRISPR/Cas9 Target Prediction Tool. *PLoS One* **10**, e0124633 (2015).

103. Krzic, U., Gunther, S., Saunders, T. E., Streichan, S. J. & Hufnagel, L. Multiview light-sheet microscope for rapid in toto imaging. *Nat Methods* **9**, 730–3 (2012).

104. Bulik-Sullivan, B. K. *et al.* LD Score regression distinguishes confounding from polygenicity in genome-wide association studies. *Nat Genet* **47**, 291–295 (2015).

105. MacArthur, J. *et al.* The new NHGRI-EBI Catalog of published genome-wide association studies (GWAS Catalog). *Nucleic Acids Res* **45**, D896–D901 (2017).

106. Stanescu, H. C. *et al.* Risk HLA-DQA1 and PLA(2)R1 alleles in idiopathic membranous nephropathy. *N Engl J Med* **364**, 616–26 (2011).

107. Almoguera, B. *et al.* Identification of Four Novel Loci in Asthma in European American and African American Populations. *Am J Respir Crit Care Med* **195**, 456–463 (2017).

108. Kunz, M. *et al.* Genome-wide association study identifies new susceptibility loci for cutaneous lupus erythematosus. *Exp Dermatol* **24**, 510–5 (2015).

109. Ligthart, S. *et al.* Bivariate genome-wide association study identifies novel pleiotropic loci for lipids and inflammation. *BMC genomics* **17**, 443–443 (2016).

110. Kanai, M. *et al.* Genetic analysis of quantitative traits in the Japanese population links cell types to complex human diseases. *Nat Genet* **50**, 390–400 (2018).

111. Wild, P. S. *et al.* Large-scale genome-wide analysis identifies genetic variants associated with cardiac structure and function. *J Clin Invest* **127**, 1798–1812 (2017).

112. Roselli, C. *et al.* Multi-ethnic genome-wide association study for atrial fibrillation. *Nat Genet* **50**, 1225–1233 (2018).

113. Tereshchenko, L. G. *et al.* Genome-Wide Associations of Global Electrical Heterogeneity ECG Phenotype: The ARIC (Atherosclerosis Risk in Communities) Study and CHS (Cardiovascular Health Study). *J Am Heart Assoc* **7** (2018).

114. van der Harst, P. *et al.* 52 Genetic Loci Influencing Myocardial Mass. *J Am Coll Cardiol* **68**, 1435–1448 (2016).

115. Evans, D. S. *et al.* Fine-mapping, novel loci identification, and SNP association transferability in a genome-wide association study of QRS duration in African Americans. *Hum Mol Genet* **25**, 4350–4368 (2016).

116. Verweij, N. *et al.* Genetic determinants of P wave duration and PR segment. *Circ Cardiovasc Genet* **7**, 475–81 (2014).

117. Pfeufer, A. *et al.* Genome-wide association study of PR interval. *Nat Genet* **42**, 153–9 (2010).

118. Dina, C. *et al.* Genetic association analyses highlight biological pathways underlying mitral valve prolapse. *Nat Genet* **47**, 1206–11 (2015).

119. Ehret, G. B. *et al.* Genetic variants in novel pathways influence blood pressure and cardiovascular disease risk. *Nature* **478**, 103–9 (2011).

120. Ehret, G. B. *et al.* The genetics of blood pressure regulation and its target organs from association studies in 342,415 individuals. *Nat Genet* **48**, 1171–1184 (2016).

121. Surendran, P. *et al.* Trans-ancestry meta-analyses identify rare and common variants associated with blood pressure and hypertension. *Nat Genet* **48**, 1151–1161 (2016).

122. Wain, L. V. *et al.* Genome-wide association study identifies six new loci influencing pulse pressure and mean arterial pressure. *Nat Genet* **43**, 1005–11 (2011).

123. Wain, L. *et al.* Novel Blood Pressure Locus and Gene Discovery Using Genome-Wide Association Study and Expression Data Sets From Blood and the Kidney. *Hypertension (Dallas, Tex. : 1979)* (2017).

124. Sotoodehnia, N. *et al.* Common variants in 22 loci are associated with QRS duration and cardiac ventricular conduction. *Nat Genet* **42**, 1068–76 (2010).

2.1 Supplementary Tables

Supplementary Table 1. Single-trait heritability estimates and genomic control All estimates based on summary statistics (t statistic) of univariate association results of 14,134,301 genetic variants and 18,096 samples. Estimates are obtained via LD score regression. Heritability estimates (h_2 are on the observed scale. Mean χ^2 is the mean χ^2 statistic. λ_{GC} is the $\frac{\text{median}\chi^2}{0.4549}$. Intercept is the LD Score regression intercept. Ratio is $\frac{\text{Intercept}-1}{\text{Mean}\chi^2-1}$. The intercept should be close to 1. The ratio measures the proportion of the inflation in the mean χ^2 that the LD Score regression intercept ascribes to causes other than polygenic heritability. The value of ratio should be close to zero, though in practice values of 10-20% are not uncommon. SE indicates the standard error. For details see: https://github.com/bulik/ldsc/wiki/Heritability-and-Genetic-Correlation and[90,104]

Slice	h_2	h_2 SE	Mean χ^2	λ_{GC}	Intercept	Intercept SE	Ratio	Ratio SE
1	0.1339	0.0316	1.0481	1.0557	0.9995	0.0072	Ratio < 0	-
2	0.1482	0.0514	1.0538	1.0436	0.9989	0.0104	Ratio < 0	-
3	0.1732	0.0345	1.0688	1.0496	1.0065	0.0074	0.0949	0.1077
4	0.1546	0.0305	1.0641	1.0557	1.0092	0.0068	0.1438	0.1058
5	0.2125	0.0313	1.0817	1.0649	1.0055	0.0071	0.0676	0.0867
6	0.2187	0.032	1.0873	1.0679	1.0095	0.0069	0.1091	0.0786
7	0.2212	0.03	1.0823	1.0679	1.0036	0.0065	0.0442	0.079
8	0.2001	0.0287	1.0723	1.0618	1.0014	0.0066	0.019	0.091
9	0.1236	0.0265	1.0433	1.0436	0.9994	0.0063	Ratio < 0	-

Supplementary Table 2. UK Biobank replication. SNP with lowest meta-analysis p-value (uncorrected for multiple comparisons) per locus in the discovery cohort (SNP and P-value discovery, see Supplementary Table 5) and the p-values of the same SNP and SNP with lowest p-value in that locus ($r^2 > 0.8$) for the replication cohort. Meta-analysis p-values were estimated based on the transformation of the univariate signed t-statistics (associations on 1,199 genetic variants at 16 independent loci from 6,536 samples) and χ^2 distribution with 9 degrees of freedom. Eight loci replicate with Bonferroni corrected threshold for the number of loci tested (n=16): $p < 0.05/16 = 0.003$.

CHR	SNP	BP	P-value discovery	Replication	
				P-value SNP	P-value locus
1	rs6587924	61895257	1.57E-17	3.40E-05	1.56E-05
1	rs35770803	155962067	3.71E-08	4.96E-01	4.96E-01
1	rs1892027	201332020	2.01E-08	3.93E-04	3.92E-04
2	rs71394376	179531078	1.40E-09	2.15E-02	7.85E-03
3	rs4677294	73554922	2.61E-16	5.21E-02	1.44E-02
3	rs1918978	169191428	2.40E-08	8.57E-03	8.57E-03
5	rs10076436	153871841	4.90E-10	4.03E-02	3.53E-02
6	rs3130976	31081940	5.29E-09	1.38E-01	7.32E-02
6	rs9320648	118690014	1.67E-17	3.35E-02	3.35E-02
8	rs6981461	11794962	1.64E-10	1.73E-07	8.06E-08
8	rs35006907	125859817	9.55E-11	8.53E-05	6.59E-05
12	rs7132327	115381071	1.97E-09	1.21E-09	1.87E-10
14	rs71105784	71990847	2.63E-11	3.45E-04	1.86E-04
17	rs17608766	45013271	1.98E-26	4.04E-09	8.75E-10
19	rs113394178	7581244	3.81E-10	3.21E-04	1.30E-04
22	rs3788488	33127481	2.81E-08	4.29E-02	4.29E-02

Supplementary Table 3. UK Biobank replication locus details. SNP identifier and chromosomal position of SNP with lowest meta-analysis p-value (not adjusted for multiple comparisons) in locus used for replication; see Supplementary Table 2). Meta-analysis p-values were estimated based on the transformation of the univariate signed t-statistics (associations on 1,199 genetic variants at 16 independent loci from 6,536 samples) and χ^2 distribution with 9 degrees of freedom.

CHR	SNP	BP	Replication P-value locus
1	rs9436640	61895257	1.56E-05
1	rs35770803	155962067	4.96E-01
1	rs1104859	201332020	3.92E-04
2	rs2042995	179531078	7.85E-03
3	rs34210879	73554922	1.44E-02
3	rs1918978	169191428	8.57E-03
5	rs13185595	153871841	3.53E-02
6	rs548139121	31081940	7.32E-02
6	rs9320648	118690014	3.35E-02
8	rs60902764	11794962	8.06E-08
8	rs7461129	125859817	6.59E-05
12	rs61933462	115381071	1.87E-10
14	rs61991243	71990847	1.86E-04
17	rs11874	45013271	8.75E-10
19	rs644053	7581244	1.30E-04
22	rs3788488	33127481	4.29E-02

Supplementary Table 4. UK Digital Heart study replication. SNP identifier and chromosomal position of SNP with lowest meta-analysis p-value in discovery (not adjusted for multiple comparisons, see Supplementary Table 5) and the p-values of the same SNP for the UK Digital Heart study replication cohort. Meta-analysis p-values were estimated based on the transformation of the univariate signed t-statistics (associations on 1,015 genetic variants at 16 independent loci from 1,136 samples) and χ^2 distribution with 9 degrees of freedom. Two loci replicate at Bonferroni corrected threshold for the number of loci tested (n=16): $p < 0.05/16 = 0.003$. One SNP was not genotyped this replication cohort (indicated by NA).

CHR	SNP	BP	P-value discovery	P-value Replication
1	rs6587924	61895257	1.57E-17	6.04E-01
1	rs35770803	155962067	3.71E-08	2.73E-01
1	rs1892027	201332020	2.01E-08	2.97E-01
2	rs71394376	179531078	1.40E-09	NA
3	rs4677294	73554922	2.61E-16	9.16E-01
3	rs1918978	169191428	2.40E-08	9.11E-03
5	rs10076436	153871841	4.90E-10	1.51E-01
6	rs3130976	31081940	5.29E-09	3.29E-01
6	rs9320648	118690014	1.67E-17	7.12E-01
8	rs6981461	11794962	1.64E-10	2.43E-02
8	rs35006907	125859817	9.55E-11	6.50E-03
12	rs7132327	115381071	1.97E-09	3.21E-01
14	rs71105784	71990847	2.63E-11	1.57E-01
17	rs17608766	45013271	1.98E-26	6.74E-01
19	rs113394178	7581244	3.81E-10	3.80E-01
22	rs3788488	33127481	2.81E-08	5.17E-02

Supplementary Table 5. Characteristics of trabeculation-associated loci. Overview of the 16 independent loci discovered in the trabeculation GWAS. The genetic variant with the lowest meta-analysis p-value (not adjusted for multiple testing) per locus is shown. Chromosomes (CHR), base pair positions (BP), ID, Locus and Type based on GRCh37 (Ensembl GRCh37 Release 95). Allele frequency (AF), reference (A_0) and alternative allele (A_1) based on discovery cohort data. INFO denotes the imputation quality score of impute2[81]. Slice indicates the slices associated with this locus, where multi denotes association in mult-variate test only. No entry indicated by -. Meta-analysis p-values were estimated based on the transformation of the univariate signed t-statistics (associations on 14,134,301 genetic variants at 16 independent loci from 18,096 samples) and χ^2 distribution with 9 degrees of freedom.

CHR	SNP	BP	A_0	A_1	AF	INFO	P	Ensembl ID	Locus	Type	Slice
1	rs6587924	61895257	C	A	0.51	1.00	1.57E-17	ENSG00000162604	TM2D1	intron	4,5,6,7
1	rs35770803	155962067	G	GT	0.63	0.96	3.71E-08	ENSG00000224276	RP11-336K24.5	intron	multi
1	rs1892027	201332020	T	C	0.71	1.00	2.01E-08	ENSG00000118194	TNNT2	intron	multi
2	rs71394376	179531078	A	AATGT	0.21	1.00	1.40E-09	ENSG00000155657	TTN	intron	3,4
3	rs4677294	73554922	T	A	0.36	0.99	2.61E-16	ENSG00000121440	PDZRN3	intron	2,3
3	rs1918978	169191428	A	G	0.58	0.98	2.40E-08	ENSG00000085276	MECOM	intron	7,8
5	rs10076436	153871841	C	G	0.36	1.00	4.90E-10	intergenic	-	-	3,4
6	rs3130976	31081940	T	C	0.29	1.00	5.29E-09	intergenic	-	-	5,6,8
6	rs9320648	118690014	A	C	0.58	1.00	1.67E-17	intergenic	-	-	5,6,7,8
8	rs6981461	11794962	T	C	0.44	0.98	1.64E-10	intergenic	-	-	multi
8	rs35006907	125859817	C	A	0.31	0.99	9.55E-11	ENSG00000255080	RP11-1082L8.3	intron	5,6
12	rs7132327	115381071	T	C	0.27	1.00	1.97E-09	intergenic	-	-	4,5
14	rs71105784	71990847	C	CCTGT	0.25	1.00	2.63E-11	intergenic	-	-	3,4
17	rs17608766	45013271	T	C	0.15	1.00	1.98E-26	ENSG00000108433	GOSR2	3'UTR intron	2,3,4
19	rs113394178	7581244	C	A	0.61	0.96	3.81E-10	ENSG00000198816	ZNF358	intron	4,5,6
22	rs3788488	33127481	T	C	0.27	0.99	2.81E-08	ENSG00000100234	TIMP3	intron	multi

Supplementary Table 6. Loci annotation in published GWAS. Based on entries in the GWAS catalogue[105]. P-values are meta-analysis p-values, not adjusted for multiple testing derived from the transformation of the univariate signed t-statistics (associations on 14,134,301 genetic variants at 16 independent loci from 18,096 samples) and χ^2 distribution with 9 degrees of freedom. No entry indicated by -. BP, Blood pressure; LV, left ventricle/left ventricular; AA, atrial appendage; CLE, Cutaneous lupus erythematosus.

CHR	BP	SNP	P	GWAS	Slice	Region
6	31081940	rs3130976	5.29E-09	Nephropathy[106], adult asthma[107], CLE[108]	5, 6, 7	mid/apical
8	11794962	rs6981461	1.64E-10	C-reactive protein[109]	multi-trait	-
8	125859817	rs35006907	9.55E-11	Ejection fraction, fractional shortening, LV internal dimension in systole and diastole, relative wall thickness[110], LV internal dimension[111], atrial fibrillation[112]	5, 6	mid
12	115381071	rs7132327	1.97E-09	Global electrical heterogeneity phenotypes[113], QRS complex[114], QRS duration[114,115], PR segment[116], PR interval[117]	4	mid
14	71990847	rs71105784	2.63E-11	QRS complex[114], QRS duration[114,115], mitral valve prolapse[118]	3, 4	basal/mid
17	45013271	rs17608766	1.98E-26	Systolic blood pressure[119–123], QRS duration[114,124], pulse and blood pressure[123], aortic root size[111], atrial fibrillation[112]	2, 3, 4	basal/mid

Supplementary Table 7. Finite element modelling. Steady-state measurements of the left ventricle obtained after 5 cardiac cycles, selectively varying only trabecular complexity, at constant total myocardial mass with identical boundary conditions.

Haemodynamics	Smooth model	Trabeculated model
Peak systolic pressure (mmHg)	93	123.6
End-systolic pressure (mmHg)	88	119.8
Diastolic pressure (mmHg)	50	65.9
Left ventricular volumes and function		
End-diastolic volume (ml)	114.8	160.4
End-systolic volume (ml)	54.8	80.1
Stroke volume (ml)	60	80.3
Stroke work (J)	0.62	1.09
Cardiac output (l/min)	3.6	4.8
Contractility (mmHg/ml)	1.61	1.50
Mass (g)	97.7	97.7

Supplementary Table 8. Disease association of NFIA (chr1) and GOSR2 (chr17) loci. rs17608766 and rs6587924 are associated with decreased trabeculation in the mid and basal regions of the heart (Supplementary Table 5 and 5). Regression of these variants or a variant in LD (LD proxy with LD r^2 as in 1000 Genomes GBR population) on heart failure (HERMES consortium[91]) and dilated cardiomyopathy show an increased disease risk for these loci with increased beta (HERMES) and increased odds ratio (OR; marked with *). Allele frequencies (AF), Odds ratios (OR), effect sizes (BETA) with respect to the A_1 allele, i.e. frequency or effect of having an extra copy of A_1. p-value is the p-value from the association test, N the number of individuals in the study, BF the Bonferroni-corrected p-value for the number of tests conducted. For UK Biobank discovery cohort p-values adjusted for the effective number of univariate associations $T_{eff} = 6.6$, for disease associations the number of loci tested: $T_{eff} = 16$. For details see Methods.

Locus	Cohort	Variant/LD proxy	LD r^2	A_0	A_1	AF	Beta/OR	SE	p-value	BF	N
chr1:61895257	UKB Discovery	rs6587924	-	C	T	0.5	-0.08	0.010	5.3E-15	3.5E-14	18,097
	HERMES	rs1997997	0.8	G	A	0.51	0.03	0.009	2.5E-03	4.0E-02	587,821
chr17:45013271	UKB Discovery	rs17608766	-	T	C	0.15	-0.07	0.011	1.7E-11	1.1E-10	18,097
	HERMES	rs17608766	-	T	C	0.14	0.04	0.011	2.2E-04	3.6E-03	955,712
	DCM	rs145153053	0.7	A	G	0.18	1.388	0.095	4.1E-04	6.6E-03	1,627

Supplementary Table 9. Mendelian randomisation results for FD associations with mixed aetiology heart failure and dilated cardiomyopathy. nsnp specifies the number of snps present in both the exposure (FD associations) and outcome study. b and se are the causal effect size estimate and standard error of the study and MR method, pval the p-value of the MR analysis (not adjusted for multiple testing) as specified in the 'methods' column. For MR Egger, the magnitude of dilution bias is $I^2 = 0.98368$ and $I^2 = 0.9830075$, i.e. an approximately 1.6% and 1.7% underestimation of effect size is expected for DCM and mixed aetiology heart failure MR, respectively. F statistics and their lower bound can be found in Supplementary Table 11. For details on methods and statistics refer to Supplementary Note 1.1: Mendelian randomisation.

outcome	method	nsnp	b	se	pval
Heart failure - HERMES	MR Egger	12	-0.4978	0.174188655	0.017020598
Heart failure - HERMES	Inverse variance weighted	12	-0.11488	0.048131871	0.016994636
Heart failure - HERMES	Weighted median	12	-0.10535	0.047411945	0.026284417
Heart failure - HERMES	Weighted mode	12	-0.16451	0.07156832	0.042129831
Dilated cardiomyopathy	MR Egger	11	-2.21315	1.450045582	0.161287259
Dilated cardiomyopathy	Inverse variance weighted	11	-1.00316	0.343880362	0.003532274
Dilated cardiomyopathy	Weighted median	11	-0.93172	0.450643115	0.038683286
Dilated cardiomyopathy	Weighted mode	11	-1.05602	0.608401076	0.113262308

Supplementary Table 10. Steiger directionality analysis for causality of trabecular complexity with heart failure and dilated cardiomyopathy. snp r2.exposure and snp r2.outcome are the r^2 estimates of the correlation of all instrumental variables with the exposure and outcome traits, respectively. snp r2.exposure differ dependent on how many genetic variants overlapped between the FD associations and the outcome study - correlation only estimated for variants present in outcome and exposure. correct specifies if the hypothesised direction of FD upstream of the outcome trait is true. The p-values (steiger pval) were estimated using the MR Steiger test. For details on MR Steiger refer to Mendelian randomisation.

outcome	snp r2.exposure	snp r2.outcome	correct causal direction	steiger pval
Heart failure - HERMES	0.035811917	5.39E-05	TRUE	1.97E-132
Dilated cardiomyopathy	0.03380195	0.007333759	TRUE	0.000119535

Supplementary Table 11. F statistic of MR studies. The F statistic depends on the sample size in the exposure study (N exposure), number of IVs (IV), and the proportion of variance in the risk factor explained by the IVs (r2). It is computed by $\frac{r^2 \times (\text{N exposure} - 1 - \text{IV})}{(1-r^2) \times \text{IV}}$. As the F statistic is a cohort estimate of the unknown population F parameter a lower bound of the F parameter (F_{lower}) was estimated according to [58, Appendix A3]. All lower bounds are ≥ 10, so no strong weak instrument bias would be expected Mendelian randomisation.

outcome	IV	N exposure	N outcome	r2 exposure	F statistic	Lower bound F
Heart failure - HERMES	12	18097	589093	0.035811917	55.97306169	48.98868669
Dilated cardiomyopathy	11	18097	1628	0.03380195	57.5176894	50.1270644

Supplementary Table 12. Pleiotropy assessment with MR-Egger for FD associations. Pleiotropy assessments are shown for analysis of mixed aetiology heart failure and DCM as outcomes. egger intercept and se are the pleiotropy estimate and its standard error, pval the p-pvalue of the intercept. All statistics were estimated by MR Egger. For details on MR Egger refer to Mendelian randomisation.

outcome	egger intercept	se	pval
Heart failure - HERMES	0.033338577	0.014738401	0.047206158
Dilated cardiomyopathy	0.105545727	0.122876293	0.412655488

Supplementary Table 13. Cardiac and cardiovascular LDhub traits. Manual selection of all LDhub traits related to cardiac phenotypes and cardiovascular diseases. Used for genetic correlation analysis with trabeculation phenotypes depicted in Extended Data Fig 7f,g.

Original LDhub label	Short names
Diastolic blood pressure_automated reading	Diastolic blood pressure
Systolic blood pressure_automated reading	Systolic blood pressure
Pulse rate	Pulse rate
Pulse wave reflection index	Pulse wave reflection index
Pulse wave peak to peak time	Pulse wave peak to peak time
Target heart rate achieved	Target heart rate achieved
Pulse wave Arterial Stiffness index	Pulse wave Arterial Stiffness Index
Non-cancer illness code_self-reported: hypertension	self-reported: hypertension
Non-cancer illness code_self-reported: angina	self-reported: angina
Non-cancer illness code_self-reported: heart attack/myocardial infarction	self-reported: heart attack/myocardial infarction
Non-cancer illness code_self-reported: hypertrophic cardiomyopathy (hcm / hocm)	self-reported: hypertrophic cardiomyopathy
Illnesses of father: Heart disease	Illnesses of father: Heart disease
Illnesses of father: High blood pressure	Illnesses of father: High blood pressure
Illnesses of father: Diabetes	Illnesses of father: Diabetes
Illnesses of mother: Heart disease	Illnesses of mother: Heart disease
Illnesses of mother: High blood pressure	Illnesses of mother: High blood pressure
Illnesses of siblings: Heart disease	Illnesses of siblings: Heart disease
Illnesses of siblings: High blood pressure	Illnesses of siblings: High blood pressure
Vascular/heart problems diagnosed by doctor: Heart attack	diagnosed by doctor: Heart attack
Vascular/heart problems diagnosed by doctor: None of the above	diagnosed by doctor: Vascular/heart problems
Vascular/heart problems diagnosed by doctor: Angina	diagnosed by doctor: Angina
Vascular/heart problems diagnosed by doctor: High blood pressure	diagnosed by doctor: High blood pressure
Medication for cholesterol_blood pressure_diabetes_or take exogenous hormones: Blood pressure medication	Medication (1) : Blood pressure medication
Medication for cholesterol_blood pressure or diabetes: Blood pressure medication	Medication (2): Blood pressure medication
Diagnoses - main ICD10: I20 Angina pectoris	ICD10: I20 Angina pectoris
Diagnoses - main ICD10: I21 Acute myocardial infarction	ICD10: I21 Acute myocardial infarction
Diagnoses - main ICD10: I25 Chronic ischaemic heart disease	ICD10: I25 Chronic ischaemic heart disease
Diagnoses - main ICD10: I30 Acute pericarditis	ICD10: I30 Acute pericarditis
Diagnoses - main ICD10: I48 Atrial fibrillation and flutter	ICD10: I48 Atrial fibrillation and flutter

Supplementary Table 14. Trabeculation-associated variants and LD proxies. Statistics and summaries for LD proxies of associated variants. Cluster plots of the variants or their LD proxies are depicted in Supplementary Fig 1.

			LD proxy			
chr	rsID	BP	rID	BP	p-value	r^2
1	rs6587924	61895257	rs2207790	61897967	1.65E-15	0.84
1	rs35770803	155962067	rs12043212	155964698	6.08E-06	0.58
1	rs1892027	201332020	rs3729547	201334382	2.92E-08	0.97
2	rs71394376	179531078	rs2042995	179558366	1.35E-08	0.92
3	rs4677294	73554922	rs7647178	73565183	1.04E-13	0.86
3	rs1918978	169191428	rs7613621	169191186	3.81E-07	0.54
5	rs10076436	153871841	rs10054375	153871832	6.94E-10	1
6	rs3130976	31081940	rs3095298	31082932	1.21E-08	0.97
6	rs9320648	118690014	rs6569015	118686344	2.54E-14	0.96
8	rs6981461	11794962	rs60176945	11796674	1.03E-09	0.91
8	rs35006907	125859817	rs12542527	125876444	1.94E-08	0.86
12	rs7132327	115381071	rs10850409	115381740	6.47E-09	1
14	rs71105784	71990847	rs72728427	71769989	1.53E-10	1
17	rs17608766	45013271	-	-	-	genotyped
19	rs113394178	7581244	rs4804662	7575408	6.46E-02	0.26
22	rs3788488	33127481	rs2413146	33125992	1.55E-07	0.76

Supplementary Table 15. Material parameters in the computational model strain energy function.

Material parameter	**Diastolic Value**	**Maximum systolic value**
C_{10} (kPa)	0.2	7.2
k_1 (kPa)	1	180
k_2 (-)	2	2

Supplementary Table 16. Resistances, compliance and atrial pressures in the *in silico* model pre-load and after-load circuits. Compare to Extended Data Fig 7c.

$\mathbf{P}_{LA}$ (mmHg)	$\mathbf{R}_1$ (mmHg*min/l)	$\mathbf{R}_2$ (mmHg*min/l)	$\mathbf{R}_3$ (mmHg*min/l)	**C** (l/mmHg)	$\mathbf{P}_{RA}$ (mmHg)
5.25	0.2	0.375	18	0.0012	5

Supplementary Table 17. CRISPR target sites for allelic series in medaka. PAM sites specified in brackets.

Name	Sequence
gosr2_T1	CAGGAGGTTCAGTGTCTGAT[GGG]
gosr2_T1	TTGGCGTTCTGGCGGCGATT[CGG]
gosr2_T3	ACGCTATACCAGAGAGGCGC[AGG]
gosr2_T4	AACTGCAGAGTCTCGTCAAT[GGG]
mtss1_T1	TTGCGCTGTTCAGTTGGGGC[TGG]
mtss1_T2	GATGAGGAGACGTCTATGTT[AGG]
mtss1_T3	GATCTGAAGGCCTCAGACTA[TGG]
tnnt2a_T1	GGACATCCATCGTAAGAGAA[TGG]
tnnt2a_T2	AGAGCGCCAAAAACGTCTTG[AGG]
tnnt2a_T3	CGAAAGAGCTCGTAAGGAAG[AGG]
tnnt2a_T4	TCAAGATAGACTTAAGTAAG[TGG]

Supplementary Table 18. Oligonucleotides for CRISPR sgRNA cloning. Oligonucleotides depicted in 5'-3'orientation.

Name	Sequence
gosr2_T1_F	TAggGGAGGTTCAGTGTCTGAT
gosr2_T1_R	AAACATCAGACACTGAACCTCC
gosr2_T2_F	TAggGGCGTTCTGGCGGCGATT
gosr2_T2_R	AAACAATCGCCGCCAGAACGCC
gosr2_T3_F	TAggGCTATACCAGAGAGGCGC
gosr2_T3_R	AAACGCGCCTCTCTGGTATAGC
gosr2_T4_F	TAggCTGCAGAGTCTCGTCAAT
gosr2_T4_R	AAACATTGACGAGACTCTGCAG
mtss1_T1_F	TAggGCGCTGTTCAGTTGGGGC
mtss1_T1_R	AAACGCCCCAACTGAACAGCGC
mtss1_T2_F	TAGgTGAGGAGACGTCTATGTT
mtss1_T2_R	AAACAACATAGACGTCTCCTCA
mtss1_T3_F	TAGgTCTGAAGGCCTCAGACTA
mtss1_T3_R	AAACTAGTCTGAGGCCTTCAGA
tnnt2a_T1_F	TAGGACATCCATCGTAAGAGAA
tnnt2a_T1_R	AAACTTCTCTTACGATGGATGT
tnnt2a_T2_F	TAgGAGCGCCAAAAACGTCTTG
tnnt2a_T2_R	AAACCAAGACGTTTTTGGCGCT
tnnt2a_T3_F	TAgGAAAGAGCTCGTAAGGAAG
tnnt2a_T3_R	AAACCTTCCTTACGAGCTCTTT
tnnt2a_T4_F	TAggAAGATAGACTTAAGTAAG
tnnt2a_T4_R	AAACCTTACTTAAGTCTATCTT

2.2 Supplementary Figures

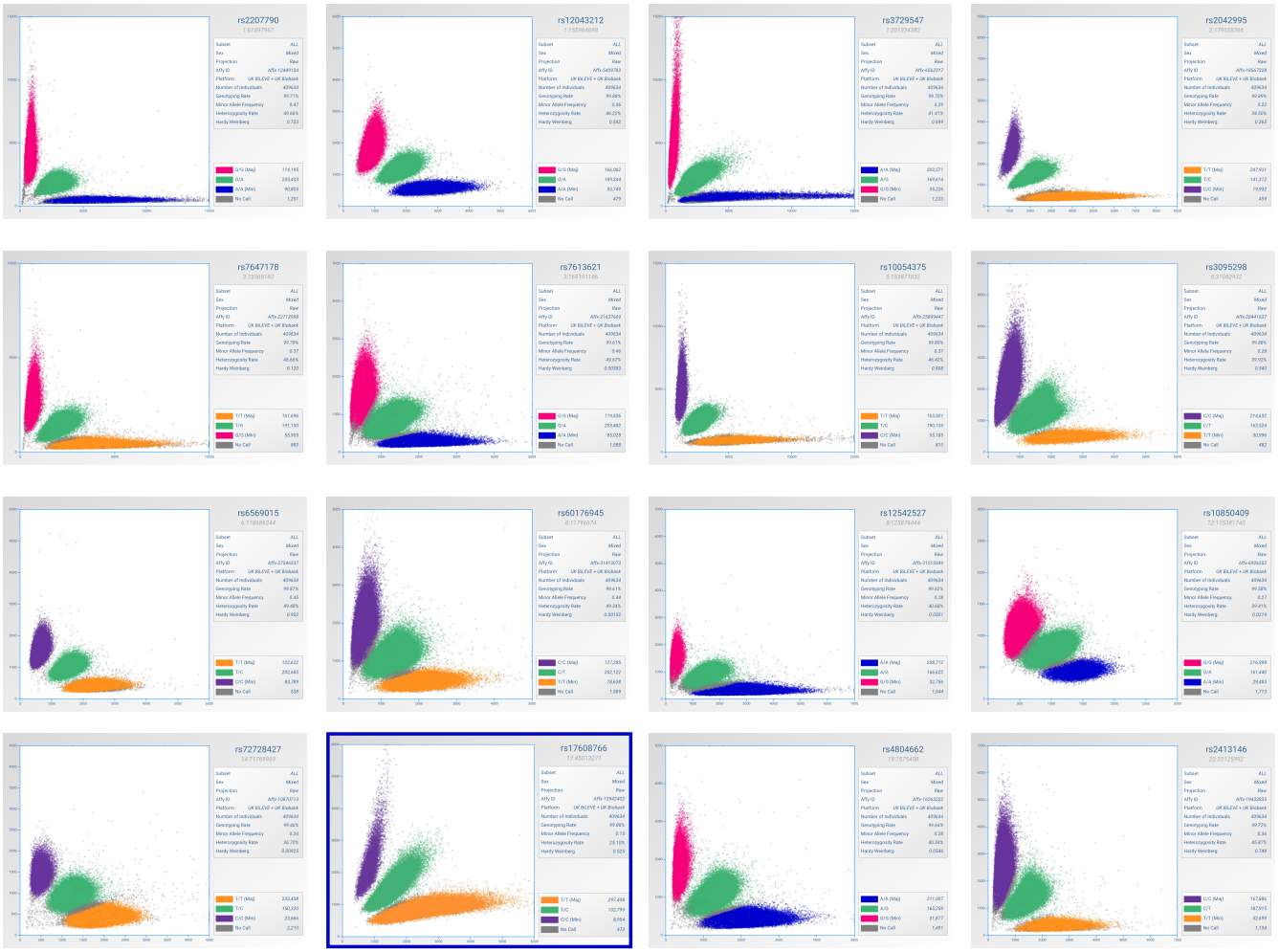

Supplementary Figure 1. Cluster plots of trabeculation-associated variants and LD proxies. Directly genotyped variants are indicated with a blue box. Cluster plots were generated via http://mccarthy.well.ox.ac.uk/static/software/scattershot/. Detailed information on LD proxies in Supplementary Table 14.